CHEMISTRY
AN ASIAN JOURNAL
ACES
COMMUNICATION

DOI: 10.1002/asia.201300717

Ta_3N_5 Nanowire Bundles as Visible-Light-Responsive Photoanodes

Cheng Hao Wu,[a] Christopher Hahn,[a] Sher Bahadar Khan,[b] Abdullah M. Asiri,[b] Salem M. Bawaked,[b] and Peidong Yang*[a, b]

Dedicated to Dr. Chunli Bai on the occasion of his 60th birthday

Solar energy is one of the most promising renewable energy sources to replace fossil fuels. Using sunlight to split water enables the storage of solar energy in the chemical bonds of hydrogen.[1,2] Since Fujishima and Honda first reported water splitting using a TiO_2 electrode,[3] metal oxides have been extensively studied as photoanodes for water oxidation.[4] However, valence bands of oxides have strong oxygen 2p character. As a result, the valence band maximum (VBM) is usually substantially lower than the water oxidation potential, which leads to a significant loss in the efficiency of the oxygen evolution reaction. To reduce this energy loss, researchers have proposed a strategy of partially or completely replacing oxygen with other anions, such as nitrogen, to raise the VBM. Using this strategy, several oxynitride/nitride semiconductors, such as $In_xGa_{(1-x)}N$,[5,6] TaON,[7–9] Ta_3N_5,[10,11] $CaTaO_2N$, and $SrNbO_2N$,[12,13] have recently been identified as promising photoanode materials. Among these semiconductors, Ta_3N_5 is attractive because of its band gap of 2.1 eV, which is similar to Fe_2O_3 (2.2 eV). This band gap can achieve a maximum solar-to-hydrogen (STH) efficiency of about 15%.[14] Also, the VBM of Ta_3N_5 is about 0.8 eV higher than the VBM of Fe_2O_3,[1,15] which could reduce efficiency losses at the photoanode. Although Ta_3N_5 has an advantageous band structure, it suffers from its chemical and functional instability in aqueous solution. One possible reason for this instability is the self-oxidation of N_3^- species from the accumulation of photo-generated holes.[9]

One-dimensional nanostructures such as nanotubes and nanowires have shown great promise for photoelectrochemical and photovoltaic applications.[6,16,17] Such structures allow minority carriers to easily migrate to the surface along the radial direction, while maintaining efficient charge collection along the longitudinal direction. There have been few reports on the successful synthesis of single crystalline one-dimensional Ta_3N_5 nanostructures. Recently, Li et al. and Zhen et al. have demonstrated the fabrication of vertically aligned Ta_3N_5 nanorod arrays with promising photoelectrochemical performance and improved stability.[18a,b] Here, we report a facile high-temperature bottom-up synthetic method for producing Ta_3N_5 nanowire bundles (NWBs), which exhibit great promise as a visible-light-responsive photoanode.

The synthesis of the Ta_3N_5 NWBs was performed in two steps (see the Supporting Information for details). The first step is a molten salt synthesis of $K_6Ta_{10.8}O_{30}$ micro/nanowires, which was modified from a previous report.[19] After cleaning the products with hot deionized water and hydrochloric acid, an insoluble white powder was obtained. Scanning electron microscopy (SEM) imaging revealed that the $K_6Ta_{10.8}O_{30}$ powder is comprised of one-dimensional structures (Figure 1a) with diameters ranging from several hundred nanometers to micrometers. The second step is the conversion from $K_6Ta_{10.8}O_{30}$ to Ta_3N_5 using a nitridation procedure. After annealing the $K_6Ta_{10.8}O_{30}$ micro/nanowires in ammonia at 900 °C for 6 h in a tube furnace, the white powder was converted into a red powder. SEM imaging of this red powder shows that the one-dimensional morphology was maintained after nitridation (Figure 1b). A closer inspection revealed a morphological change on a smaller length scale: each of the thick micro/nanowires was composed of bundles of thinner nanowires with diameters around 20 nm (Figure 1c). The absorption spectrum has an edge around 620 nm (Figure 1d), which matches the band gap of previously reported absorption measurements of Ta_3N_5.[20,21] Powder X-ray diffraction performed on the sample before and after nitridation (Figure 1e) confirmed the conversion from $K_6Ta_{10.8}O_{30}$ to Ta_3N_5.

The structure of these nanowires was further investigated by transmission electron microscopy (TEM). As the Ta_3N_5 NWBs are too thick for direct TEM imaging, we sonicated the bundles in ethanol for 10 min before drop-casting them onto a TEM grid. After sonication, while most of the bundles remained intact, several individual nanowires were found. TEM imaging (Figure 2a) confirms the observation from SEM that the thin Ta_3N_5 nanowires have diameters around 20 nm. High-resolution TEM (Figure 2b) shows the single-crystalline nature of the thin Ta_3N_5 nanowires. Based

[a] C. H. Wu, Dr. C. Hahn, Prof. Dr. P. Yang
Department of Chemistry
University of California
Berkeley, CA 94720 (USA)

[b] S. B. Khan, A. M. Asiri, S. M. Bawaked, Prof. Dr. P. Yang
Center of Excellence for Advanced Materials Research (CEAMR)
King Abdulaziz University
Jeddah 21589, P.O. Box 80203 (Saudi Arabia)
Fax: (+1) 510-642-7301
E-mail: p_yang@berkeley.edu

Supporting information for this article is available on the WWW under http://dx.doi.org/10.1002/asia.201300717.

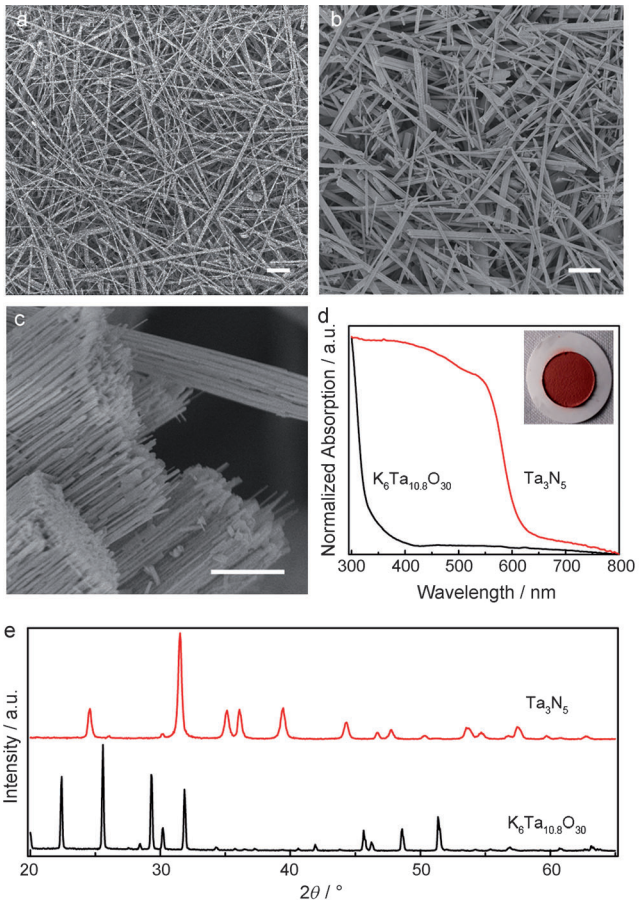

Figure 1. a) A typical SEM image of $K_6Ta_{10.8}O_{30}$ wires. b,c) Typical SEM images of Ta_3N_5 NWBs. d) Absorption spectra of $K_6Ta_{10.8}O_{30}$ wires and Ta_3N_5 NWBs. The inset shows a picture of a Ta_3N_5 nanowire bundle mesh on filter paper. e) XRD patterns before (black) and after the nitridation (red) can be assigned to $K_6Ta_{10.8}O_{30}$ (JCPDF 01-070-1088) and Ta_3N_5 (JCPDF 01-089-5200), respectively. Scale bars, 10 μm (a,b) and 1 μm (c).

on the fast Fourier transform (FFT) pattern of the high-resolution TEM image (Figure 2c) we can conclude that the longitudinal direction of the nanowire is along the *b* axis. For each of the nanowire bundles, the typical electron diffraction (ED) data show a clear single set of diffraction patterns, with bright spots elongated perpendicular to the longitudinal direction of the bundle. This suggests that the individual nanowires within these nanowire bundle are aligned along the same crystallographic directions.

A significant volume change is expected to occur during the nitridation process. Consequently, voids are being observed in the resultant nitride nanowire bundles. Intuitively, a slow temperature ramp rate can prevent a drastic change, both chemically and physically, to the $K_6Ta_{10.8}O_{30}$ crystal and suppress random void formation. In a typical reaction, the ramp rate was as slow as $2\,°C\,min^{-1}$. To demonstrate the importance of the ramp rate, control experiments were performed with fast, uncontrolled ramp rates ($>15\,°C\,min^{-1}$). The SEM images of the products show bundles of nanorods or nanoparticles instead of nanowires (Figure S1 in the Supporting Information).

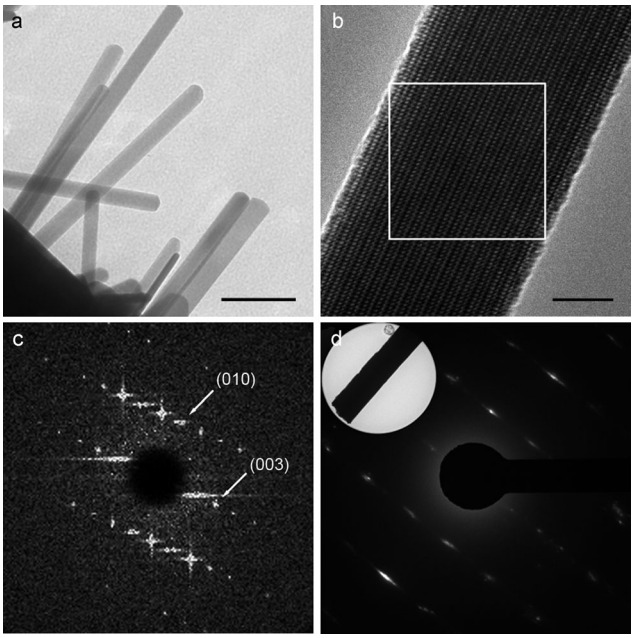

Figure 2. a) A typical TEM image of Ta_3N_5 nanowires. b) A typical high-resolution TEM image of a Ta_3N_5 nanowire. c) Fast Fourier transform (FFT) image of the white square area in the high-resolution TEM image. d) A typical electron diffraction pattern of one bundle of Ta_3N_5 nanowires. Scale bars, 100 nm (a) and 5 nm (b).

To demonstrate the photocatalytic properties of Ta_3N_5 NWBs, we used a micro gas chromatograph setup to examine the oxygen evolution under visible-light illumination ($\lambda > 400$ nm with an intensity of $75\,mW\,cm^{-2}$). Silver acetate was chosen as the electron scavenger instead of the commonly used silver nitrate, as oxidative nitrate ions may cause degradation of the nitride material. The water oxidation activity of the NWBs was compared to that of micron-sized Ta_3N_5 powders (Figure 3) which were synthesized based on a previous report.[9] More oxygen was generated from the Ta_3N_5 powder in the first 4-hour cycle. However, the performance rapidly declined in the next two cycles, which could be due to material degradation such as the for-

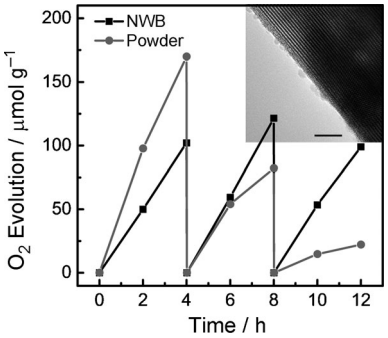

Figure 3. Oxygen evolution from Ta_3N_5 NWBs (pH ≈ 8.0, silver acetate as an electron scavenger) under visible-light illumination. The inset shows a typical high-resolution TEM image of a nanowire after the GC measurement. Silver nanoparticles, from photodeposition during the reaction, can be seen on the surface of the nanowire. Scale bar, 5 nm

mation of an oxide layer on the surface. On the other hand, the Ta_3N_5 NWBs show a relatively stable performance within the first three cycles. High-resolution TEM imaging confirmed the absence of a thick oxide layer on the nanowire surface after 12 h of illumination (inset in Figure 3). Since the crystal structure is the same for Ta_3N_5 NWBs and micro powder, the difference in stability is likely due to their different morphology. The nanoscale morphology enables the photo-generated holes to easily diffuse to the surface, thereby inhibiting self-oxidation and the formation of a thick oxide layer on the surface.

Photoelectrochemical measurements were also performed to further demonstrate the improved stability of Ta_3N_5 NWB photoanodes. Ta_3N_5 NWB electrodes were fabricated and then treated according to previous reports, with modifications (see the Supporting Information). The open-circuit potential decreased when the electrode was exposed to AM1.5G illumination (Figure 4a inset), which is characteristic for an n-type semiconductor.[2] Although the anodic photocurrent density from bare NWBs was low, it was significantly improved after loading the NWBs with an IrO_2 co-catalyst (Figure 4a). In addition, the open-circuit potential difference between dark and illumination (photovoltage) increased from 80 mV to 150 mV, and the response was faster in comparison to the bare NWBs (Figure S2 in the Supporting Information). The temporal evolution of the photocurrent density at 0.5 V versus the Ag/AgCl reference electrode (Figure 4b) also provides evidence of the improved stability of Ta_3N_5 NWBs. After exposure to illumination, both nanowire bundles and powder electrodes (both with IrO_2) show a similar spike in the photocurrent density. However, the decay rate of the NWB electrode is much slower. After 10 minutes of illumination, the photocurrent density of the Ta_3N_5 powder electrode dropped to about 30% of the original value while more than 60% of the original current density was preserved for the Ta_3N_5 NWBs electrode. This result further suggests that the improved stability is due to a more efficient diffusion of photo-generated holes to the surface.

In summary, we have demonstrated a facile two-step synthesis to produce Ta_3N_5 nanowire bundles. These thin Ta_3N_5 nanowires were single crystalline and oriented with each other to form quasi-single-crystalline nanowire bundles. Both oxygen evolution and photoelectrochemical measurements show a comparable photoanode performance for Ta_3N_5 NWBs and powders. However, NWBs possess a significantly improved stability. Future work will focus on a better understanding of the nitridation mechanism. Additional work will be done to optimize the quality and loading method of co-catalysts to further improve the performance and stability.

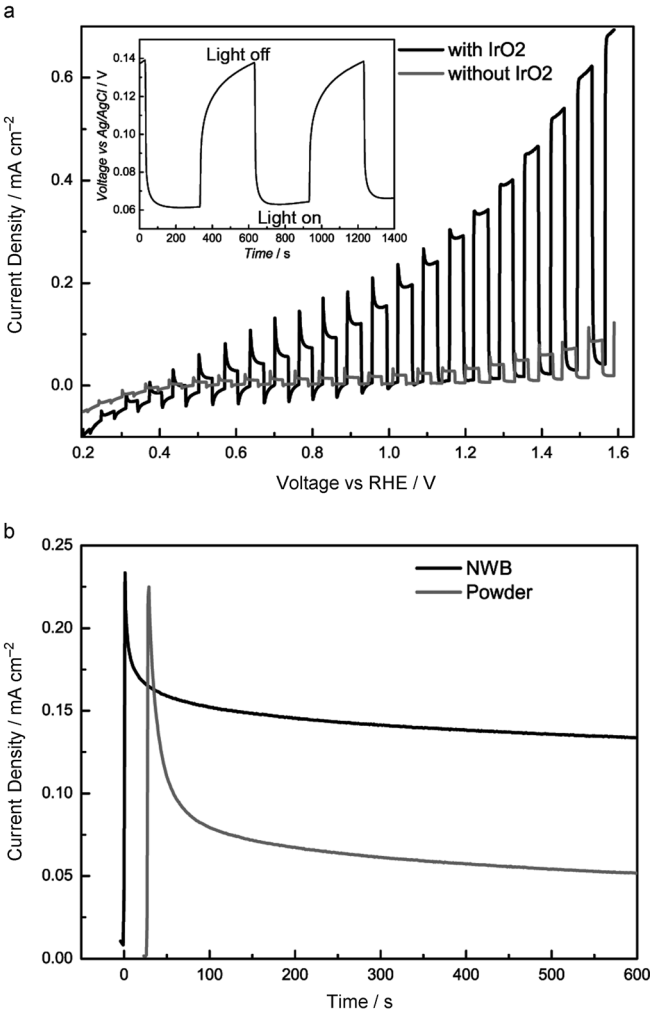

Figure 4. a) Photocurrent density of Ta_3N_5 NWB electrodes in 0.1 M Na_2SO_4 electrolyte (pH ≈ 6) under chopped AM1.5G simulated sunlight at 100 mW cm^{-2}. The inset shows the open-circuit potential change of the Ta_3N_5 NWB electrode with and without illumination. b) Time courses for the photocurrent density of the Ta_3N_5 powder electrode and the NWB electrode (both loaded with IrO_2).

Acknowledgements

We thank Dr. B. Liu and A. Fu for helpful discussions. This project was funded by the Deanship of Scientific Research (DSR), King Abdulaziz University, Jeddah, under Grant no. (HiCi/30-3-1432). The authors, therefore, acknowledge with thanks DSR technical and financial support.

Keywords: nanostructures · nitrides · photoanode · water splitting

[1] M. Grätzel, *Nature* **2001**, *414*, 338–344.
[2] M. G. Walter, E. L. Warren, J. R. McKone, S. W. Boettcher, Q. Mi, E. a. Santori, N. S. Lewis, *Chem. Rev.* **2010**, *110*, 6446–6473.
[3] A. Fujishima, K. Honda, *Nature* **1972**, *238*, 37–38.
[4] K. Rajeshwar, *J. Appl. Electrochem.* **2007**, *37*, 765–787.
[5] T. Kuykendall, P. Ulrich, S. Aloni, P. Yang, *Nat. Mater.* **2007**, *6*, 951–956.
[6] Y. J. Hwang, C. H. Wu, C. Hahn, H. E. Jeong, P. Yang, *Nano Lett.* **2012**, *12*, 1678–1682.
[7] K. Maeda, K. Domen, *MRS Bull.* **2011**, *36*, 25–31.
[8] R. Abe, M. Higashi, K. Domen, *J. Am. Chem. Soc.* **2010**, *132*, 11828–11829.

[9] M. Higashi, K. Domen, R. Abe, *Energy Environ. Sci.* **2011**, *4*, 4138.
[10] D. Yokoyama, H. Hashiguchi, K. Maeda, T. Minegishi, T. Takata, R. Abe, J. Kubota, K. Domen, *Thin Solid Films* **2011**, *519*, 2087–2092.
[11] X. Feng, T. J. Latempa, J. I. Basham, G. K. Mor, O. K. Varghese, C. a. Grimes, *Nano Lett.* **2010**, *10*, 948–952.
[12] K. Maeda, M. Higashi, B. Siritanaratkul, R. Abe, K. Domen, *J. Am. Chem. Soc.* **2011**, *133*, 12334–12337.
[13] B. Siritanaratkul, K. Maeda, T. Hisatomi, K. Domen, *ChemSusChem* **2011**, *4*, 74–78.
[14] Z. Chen, T. F. Jaramillo, T. G. Deutsch, A. Kleiman-Shwarsctein, A. J. Forman, N. Gaillard, R. Garland, K. Takanabe, C. Heske, M. Sunkara, E. W. McFarland, K. Domen, E. L. Miller, J. A. Turner, H. N. Dinh, *J. Mater. Res.* **2010**, *25*, 3–16.
[15] W. Chun, A. Ishikawa, H. Fujisawa, T. Takata, J. N. Kondo, M. Hara, M. Kawai, Y. Matsumoto, K. Domen, *J. Phys. Chem. B* **2003**, *107*, 1798–1803.
[16] Y. Hwang, C. Hahn, B. Liu, P. Yang, *ACS Nano* **2012**, *6*, 5060–5069.
[17] B. M. Kayes, H. a. Atwater, N. S. Lewis, *J. Appl. Phys.* **2005**, *97*, 114302.
[18] a) Y. Li, T. Takata, D. Cha, K. Takanabe, T. Minegishi, J. Kubota, K. Domen, *Adv. Mater.* **2013**, *25*, 125–131; b) C. Zhen, L. Wang, G. Liu, G. Q. Liu, H.-M. Chen, *Chem. Commun.* **2013**, *49*, 3019.
[19] C. Lan, J. Gong, Z. Wang, S. Yang, *Mater. Sci. Eng. B* **2011**, *176*, 679–683.
[20] K. Maeda, K. Domen, *J. Phys. Chem. C* **2007**, *111*, 7851–7861.
[21] C.-T. Ho, K.-B. Low, R. F. Klie, K. Maeda, K. Domen, R. J. Meyer, P. T. Snee, *J. Phys. Chem. C* **2011**, *115*, 647–652.

Received: May 27, 2013
Revised: June 6, 2013
Published online: July 15, 2013